Diffusion in pores and its dependence on boundary conditions

A Saugey[1], L Joly[2], C Ybert[2], J L Barrat[2] and L Bocquet[2]

[1] Laboratoire de Tribologie et Dynamique des Systèmes, Ecole Centrale de Lyon and CNRS,
36 Avenue Guy de Collongues, BP163, 69134 Ecully Cedex, France
[2] Laboratoire de Physique de la Matière Condensée et Nanostructures, Université Claude Bernard
Lyon I and CNRS, 6 rue Ampère, 69622 Villeurbanne Cedex, France

Abstract
We study the influence of the boundary conditions at the solid–liquid interface
on diffusion in a confined fluid. Using a hydrodynamic approach, we compute
numerical estimates for the diffusion of a particle confined between two planes.
Partial slip is shown to significantly influence the diffusion coefficient near
a wall. Analytical expressions are derived in the low and high confinement
limits, and are in good agreement with numerical results. These calculations
indicate that diffusion of tagged particles could be used as a sensitive probe of
the solid–liquid boundary conditions.

(Some figures in this article are in colour only in the electronic version)

1. Introduction

The no-slip boundary condition for a fluid near a solid surface is still under debate [1, 2]. At
the macroscopic scale, the no-slip boundary condition is a consequence of the microscopic
roughness [3]. On the nanometre scale, however, partial slip is possible, and has indeed been
measured experimentally [4]. This issue, which is important both fundamentally and for the
conception of microfluidic devices, has motivated a number of theoretical [5, 6] and numerical
studies [7]. These studies have highlighted the influence of the fluid–wall interaction and
pressure on the slippage [8–10]. While chemical heterogeneities and surface roughness are
expected to decrease slippage [11], surfaces with special geometries can exhibit a 'super-
hydrophobic' state with a strongly increased slippage at the surface [12, 13] that makes fluid
dynamics at solids surfaces very sensitive to surface imperfections. Such effects have been
evidenced using micro-engineered surfaces in [14].

Slippage is usually accounted for in terms of an extrapolation length, the so-called slip
length, here denoted as δ [5]. This is defined as the distance inside the solid wall where the

extrapolated flow profile vanishes. More specifically this partial slip boundary condition is written, for the tangential component, v_t, of the velocity as

$$v_t = \delta \frac{\partial v_t}{\partial n} \tag{1}$$

with n the coordinate in the direction normal to the solid surface. The precise value of this slip length and its dependence on the physical and chemical characteristics of the surface have been investigated in a number of recent experimental studies. In particular, very different values for slip lengths—from a few nanometres to microns—have been reported using different techniques (see e.g. [4] for a review). Many of these techniques are indirect (pressure drop measurements [10, 14], particle image velocimetry [15], fluorescence recovery [11]), or very delicate (surface force apparatus [2] and atomic force microscopy [16]). Hence the development of complementary, robust and non-intrusive techniques to investigate the dynamical properties of the solid–liquid interface would provide valuable counterparts of the previous results.

In this manuscript, we discuss how the diffusion of tagged particles between walls is affected by confinement, and how such measurements could be used as a signature of the nature of the boundary conditions [17–19].

We develop a theoretical and numerical approach to estimate the roles of confinement and slip on diffusion constrained in a planar or cylindrical pore. We make use of a classical hydrodynamic description, which is expected to be appropriate for colloidal particles, and was previously shown to be also well adapted for molecular diffusion [5]. A numerical approach is used for the general case, and analytical expressions are derived in the high and low confinement regimes.

2. Hydrodynamic estimate of the diffusion constant

The quantity of interest is the mean diffusion coefficient of colloidal tracers averaged over the measurement volume. The latter is limited here by the presence of the confining walls. From a theoretical point of view, a moving particle $\mathcal{P}$ is subjected to a friction force proportional to its velocity. When the motion takes place in a confined volume, the mobility μ depends on the boundary conditions at the confining walls. For a velocity $\underline{U}$ parallel to the boundary, the diffusion coefficient $D_\parallel$ is given by Einstein's relation [20]

$$D_\parallel = \mu k_B T. \tag{2}$$

For a particle moving between two flat walls separated by a distance H, $D_\parallel$ is a function of the particle radius a, the height H and the position z of the particle respective to the walls (in the following z will be measured by taking the origin at the midplane). The average diffusion coefficient in the direction parallel to the walls is

$$\langle D_\parallel \rangle = \frac{1}{H - 2a} \int_a^{H-a} D_\parallel(z) \, dz. \tag{3}$$

The next step is to use the so-called Stokes–Einstein approach, i.e. to estimate the friction force from hydrodynamics. At low Reynolds number, the flow around the particle is governed by the Stokes equations:

$$\eta \Delta \underline{V} = \underline{\nabla} P \tag{4}$$

$$\underline{\nabla} \cdot \underline{V} = 0 \tag{5}$$

where $\underline{V}$ is the velocity field, P the pressure field and η the viscosity of the fluid. The boundary conditions are

- fluid at rest at infinity in the unconfined directions:

$$\underline{V}\big|_{\infty} = \underline{0} \tag{6}$$

- no slip on the particle surface:

$$\underline{V}\big|_{\mathcal{P}} = \underline{U} \tag{7}$$

- partial slip on solid walls, expressed by parallel $\underline{V}_{\parallel}\big|_{\mathcal{S}}$ and perpendicular $\underline{V}_{\perp}\big|_{\mathcal{S}}$ velocities and slip length δ:

$$\delta \, \nabla_{\perp} \underline{V}_{\parallel}\big|_{\mathcal{S}} - \underline{V}_{\parallel}\big|_{\mathcal{S}} = \underline{0} \tag{8}$$

$$\underline{V}_{\perp}\big|_{\mathcal{S}} = 0. \tag{9}$$

This condition is written $\mathcal{BC}_{\mathcal{S}}(\underline{V}) = \underline{0}$.

The friction force experienced by the particle is then:

$$\underline{F} = \int\!\!\int_{\partial\mathcal{P}} \underline{\underline{\sigma}} \cdot \mathrm{d}\underline{S} \tag{10}$$

where $\underline{\underline{\sigma}} = -P\underline{\underline{I}} + \eta \left(\underline{\nabla}\,\underline{U} +^{t} \underline{\nabla}\,\underline{U} \right)$ is the stress tensor in the fluid.

In the next sections we provide various solutions to this boundary problem: we first start with a numerical 'exact' solution of these equations; the latter will be used subsequently as a reference solution for the approximate analytical solutions obtained under various assumptions.

3. Numerical estimates

In this section we first start with a numerical solution of the previous equations, equations (4)–(9). This set of equations was solved numerically with the *FEMLAB*© software. A finite domain of size $2L \times 2L \times H$ around the particle was considered (figure 1). The size L was chosen large enough compared to H to avoid finite size problems: typical values are $L/a = 20$ for small H, $L = 3H$ otherwise. Space and time symmetries were taken into account to reduce the meshed domain for faster computations.

From a technical point of view, the *FEMLAB* fluid dynamics module solves the bulk equations as

$$\underline{\nabla} \cdot \underline{\underline{\sigma}} = \underline{0} \tag{11}$$

$$\underline{\nabla} \cdot \underline{V} = 0 \tag{12}$$

with the stress tensor $\underline{\underline{\sigma}}$ given above. Boundary conditions are imposed according to equations (7)–(9).

Once the flow field has been obtained in this geometry, the force is computed according to equation (10). Note that this way of computing the force requires a fine mesh since a differentiation of the velocity field is performed. A better approach would consist in using a weak constraint formulation so that velocity and force are simultaneously computed on the surface. However, such an approach is time and memory consuming and was not used in this work to keep computational time within reasonable bounds.

Typical results are shown in figure 2, where the profile of the *local* parallel diffusion coefficient is plotted as a function of the altitude in the confining slab. As a case study, we consider the situation in which one of the two walls has a non-zero slip length, while the no-slip boundary condition is applied at the second wall. Near the no-slip wall, diffusion decreases from its bulk value as a result of the viscous friction and high velocity gradient in the fluid between the particle and the wall. This well known phenomenon [21] is easily explained in term of an image particle (see next section). For a no-slip wall, the image particle moves in
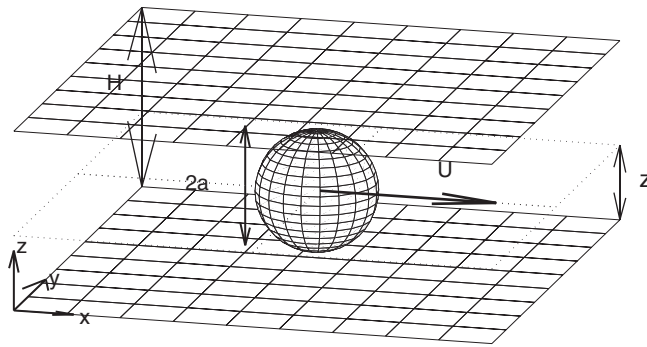
Figure 1. Geometry of the present calculations. A tracer particle with radius *a* diffuses in a slab with thickness H.
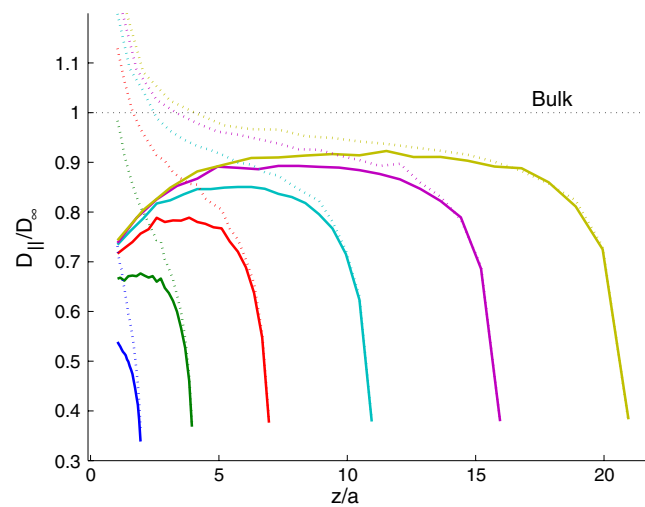

Figure 2. Numerical estimates of the reduced diffusion coefficient of a particle moving between a partially slipping wall ($\delta = 1$: full line, $\delta = 100$: dotted line) at $z = 0$ and a no-slip wall at $z = H$, as a function of the position of the particle. From left to right, $H/a = 3, 5, 8, 12, 17$ and 22.

the opposite direction thus increasing the viscous force acting on the particle. Near a partially slipping wall diffusion increases from the no-slip case and can even be higher than the bulk value. In the limit $\delta \rightarrow \infty$, diffusion reaches a high value that can be estimated using the image particle approach, with the image moving in the same direction as the particle [17].

We now turn to analytical approximate solutions of the Stokes equation in the previous geometry.

4. Analytical expressions in the low confinement (large gap) limit

When the particle is small compared to confinement height, an iterative reflection method can be developed, leading to an analytical expression for the friction force.

In the present work we use this approach in the presence of a single, slipping, wall. Then, summing over the forces due to each wall yields an approximate result for the average diffusion coefficient. A summary of the method is given here, and details are discussed in appendix A.

4.1. Reflection method with a single, slipping, wall

The reflection method is an iterative approach [21], in which the velocity field $\underline{V}$ is expanded in the form

$$\underline{V} = \underline{V}^0 + \underline{V}^1 + \underline{V}^2 + \underline{V}^3 + \cdots \tag{13}$$

with each $\underline{V}^n$ field satisfying the bulk equations (4) and (5). The zero-order field, $\underline{V}_0$, is chosen as the flow field around a sphere moving in the bulk:

$$\underline{V}^0(r, z) = \frac{3}{4} aU \left(\frac{2}{r} \underline{\nabla}(z) - \underline{\nabla}\left(\frac{z}{r}\right) + \frac{a^2}{3} \underline{\nabla}\left(\frac{z}{r^3}\right) \right) \tag{14}$$

with a the radius of the sphere. This velocity field satisfies the boundary equations on the particle (equation (7)) and at infinity (equation (6)). The method consists in determining the $\underline{V}^1$ field such that $\underline{V}^0 + \underline{V}^1$ satisfies the boundary conditions at infinity and on the solid walls (8) and (9):

$$\mathcal{BC}_{\mathcal{S}}(\underline{V}^1) = -\mathcal{BC}_{\mathcal{S}}(\underline{V}^0)$$
$$\underline{V}^1\big|_{\infty} = \underline{0}.$$

Now, at this level of approximation, the boundary condition on the particle $\mathcal{P}$ is no longer satisfied by $\underline{V}^0 + \underline{V}^1$, and the next-order $\underline{V}^2$ is defined from the reflection of $\underline{V}^1$ on the particle as

$$\underline{V}^2\big|_{\mathcal{P}} = -\underline{V}^1\big|_{\mathcal{P}}$$
$$\underline{V}^2\big|_{\infty} = \underline{0}.$$

The higher moments of the velocity field, $\underline{V}^n$, are built by applying the boundary condition iteratively on the particle and on the flat walls.

4.2. Viscous force acting on the particle: a single wall

The friction force experienced by the particle is the sum of individual contributions $\underline{F}^n$ of each reflection:

$$\underline{F}^n = \int\!\!\int_{\partial\mathcal{P}} \underline{\underline{\sigma}}^n \cdot \mathrm{d}\underline{S} = \int\!\!\int\!\!\int_{\mathcal{P}} \underline{\nabla} \cdot \underline{\underline{\sigma}}^n \mathrm{d}V \tag{15}$$

where $\underline{\underline{\sigma}}^n$ is the stress tensor in the fluid. For odd reflections, the velocity is regular in the volume of the particle. The momentum equation gives $\underline{\nabla} \cdot \underline{\underline{\sigma}}^n = 0$ in the domain occupied by $\mathcal{P}$ and the integral vanishes. For even reflections, the Lorentz reciprocal theorem [21] gives algebraically, *in the limit of small particles*, $F^{n+2} = \frac{V_{\mathcal{O}}^{n+1}}{V_{\mathcal{O}}^{n-1}} F^n$, where $V_{\mathcal{O}}^n$ is defined as the value of the velocity field at the centre of the particle. One thus obtains

$$\underline{F} = -\underline{F}^0 \sum_{k=0}^{\infty} \left[-\frac{V_{\mathcal{O}}^1}{U} \right]^k = -\frac{\underline{F}^0}{1 + \frac{V_{\mathcal{O}}^1}{U}} \tag{16}$$

with $\underline{F}^0 = 6\pi\eta a\underline{U}$. As a consequence, only the velocity of the first reflected field at the centre of the particle $V_{\mathcal{O}}^1$ is needed to determine the mobility and diffusion coefficient. The calculation of this field is described in appendix A.

Equations (16) and (A.7) give the force acting on a particle moving along a single planar wall as a function of the radius of the particle a, the distance from the wall l and the slip length δ:

$$\underline{F}_{1\text{wall}} = \frac{6\pi\eta a}{1 - \frac{a}{z} C\left[\frac{l}{\delta}\right]} \underline{U} \tag{17}$$
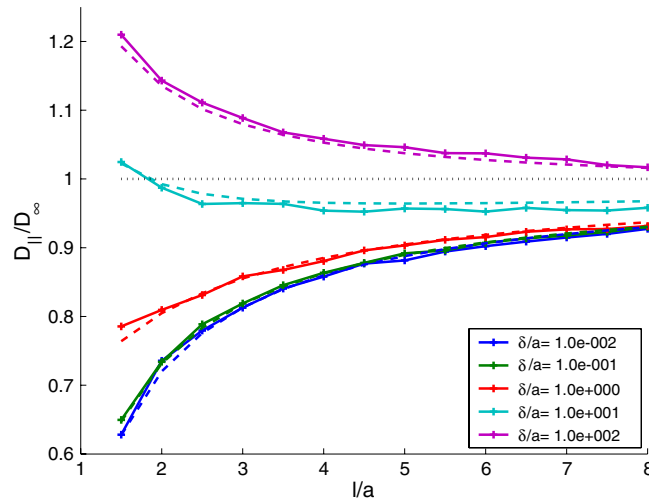
Figure 3. Diffusion coefficient near a single planar wall as a function of the distance l, for various slip length. Numerical results (solid lines) are compared with the analytical solution (dashed line) in the low confinement limit $l \gg a$. The slip length δ increases from bottom to top.

where the function C is defined as

$$C[y] = -\tfrac{3}{32}y^2 - \tfrac{9}{32}y - \tfrac{3}{8} + \left(\tfrac{3}{32}y^3 + \tfrac{3}{8}y^2 + \tfrac{3}{8}y\right) E(y) + \tfrac{3}{2}y E(2y) \tag{18}$$

with $E(y) = e^y E_1(y)$ and $E_1(y)$ is the exponential integral function, defined as $E_1(z) = \int_z^\infty dt\, e^{-t}/t$ [22].

When $\delta \to 0$ (no-slip condition), one recovers the well known value

$$C\left[\frac{l}{\delta}\right] \to \frac{9}{16} \tag{19}$$

derived from the method of the image particle [21]: as mentioned above, diffusion decreases near a no slip wall. In the limit $\delta \to \infty$ (full slip condition),

$$C\left[\frac{l}{\delta}\right] \to -\frac{3}{8} \tag{20}$$

and the presence of the wall reduces the friction force, i.e. diffusion increases, as measured experimentally [17].

Comparisons with numerical simulations using FEMLAB© are shown in figure 3. The results are in good agreement down to very small distances $l/a = 1.5$. At large distance, one recovers the bulk diffusion value, as expected.

Moreover, simple and practical approximations can be obtained for the mobility in the limit where the distance to the wall, l, is large compared to the slip length δ. Indeed an asymptotic expansion of $C[y]$ allows one to obtain

$$C[y] = \frac{9}{16}\frac{1}{1 + \frac{1}{y} + \mathcal{O}\left[\frac{1}{y^2}\right]}. \tag{21}$$

This gives the approximate following form for the friction coefficient:

$$\underline{F}_{1\text{wall}} \simeq \frac{6\pi \eta a}{1 - \frac{9}{16}\frac{a}{l+\delta}}\underline{U}. \tag{22}$$
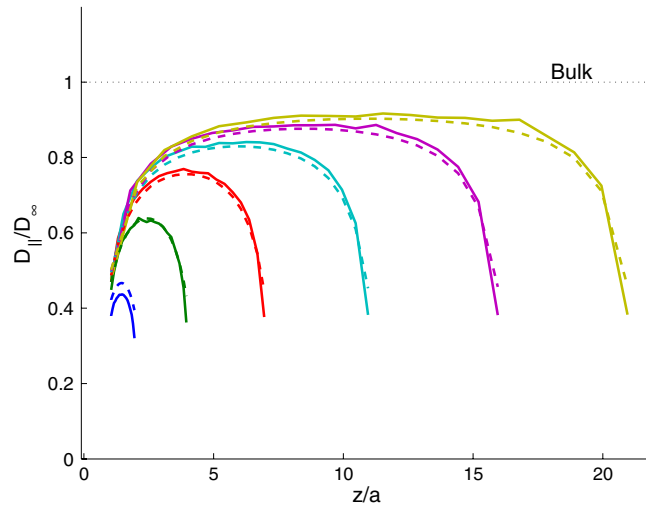
Figure 4. Local diffusivity computed using the approximate analytical results equation (24) for $\delta/a = 10^{-1}$ (dashed line), compared to the numerical results (solid line). See figure 2 for details and notations.

This approximation amounts to replacing the distance to the wall l by $l + \delta$, where the physical meaning of the slip length in terms of an extrapolation length appears quite clearly in this limit. In practice, note that the expression in equation (22) leads to values which are within 5% of the explicit result in equation (17) as soon as $l/\delta > 0.5$!

After completing this work, we became aware of a similar calculation by Lauga and Squires [23] who computed the viscous force on a spherical particle close to a wall, using the same reflection method. The use of the 'small particle' approximation corresponds to computing the flow in response to a force applied to a point-like particle, and can be shown to involve errors of order $(a/h)^3$ [23].

4.2.1. Local diffusivity in a confined geometry. In order to compute the friction coefficient for a particle confined between two planar walls, we make the further assumption that each wall contributes independently to the shift in the friction force from its bulk value:

$$\underline{F}_{2\text{walls}} = \underline{F}_{1\text{wall}}(z, \delta) + \underline{F}_{1\text{wall}}(H - z, \delta) - \underline{F}_{\text{bulk}} \tag{23}$$

where H is the distance between the two walls and here z denotes the distance to the bottom wall. The Einstein equation then yields for the parallel diffusion coefficient at a height l:

$$D_{\parallel} = \frac{k_{\text{B}}T}{6\pi \eta a U} \frac{1}{\frac{1}{1 - \frac{a}{z}C\left[\frac{z}{\delta}\right]} + \frac{1}{1 - \frac{a}{H-z}C\left[\frac{H-z}{\delta}\right]} - 1}. \tag{24}$$

This expression for the friction coefficient is checked against the 'exact' numerical results obtained using the FEMLAB software in figures 4 and 5. Over the various slip lengths δ and confinement gap H, the agreement is found to be quite good, within 6% as long as the confinement is no too strong ($h/2a > 4$). It can be observed that equation (24) slightly underestimates the diffusion.

Note that a different approximation could be made for the contribution of the two walls, by assuming that the mobility (rather than its inverse) is affected independently by the two walls [24]. This approximation, however, turns out to be less accurate than the previous approximation, in equation (24).
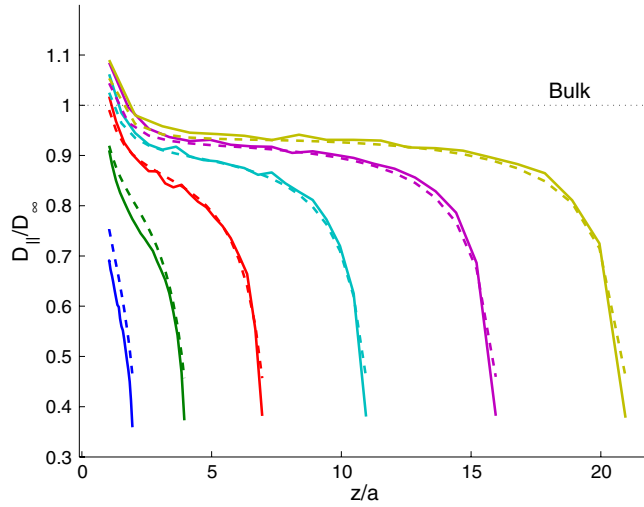
Figure 5. Same as in figure 4 but for $\delta/a = 10^1$. See figure 2 for details and notations.

When the particle is confined to a cylindrical pore, a similar method can be used and provides an estimate of the viscous force acting on the particle in the low confinement limit (see appendix A). However, as opposed to the planar case, only a numerical estimation of the reflected velocity at the centre of the sphere can be reached. An interesting difference between the planar and the cylindrical case is that in the latter case, except close to the wall where the behaviour is similar to a particle moving near a planar wall, the force acting on a tracer particle is never smaller than its bulk value even in the large slip length limit (i.e. the diffusion is reduced). This is due to the necessary recirculation of the fluid around the particle. More precisely, boundary conditions at infinity (no flow) impose the overall flow rate on a section of the cylinder at zero. In the section centred on the particle, a negative fluid flow rate has to balance the positive flow rate of the particle $\pi a^2 U$. Hence the viscous force increases from the bulk value even when $\delta \to \infty$. In the planar geometry, recirculation takes place at infinity in the unconfined directions and this phenomenon does not take place.

5. Lubrication theory in the strong confinement limit

When the confinement approaches the particle size ($H \simeq 2a$), the main part of the viscous force is expected to arise from the high velocity gradient in the thin fluid films between each wall and the particle. In these regions, the fluid flow is quasi-parallel to the wall and lubrication theory [25] is expected to provide a good description of the velocity field. An approximation of the force acting on the particle can then be derived.

We assume here that the fluid is confined between a fixed sphere and a solid wall moving at velocity $\underline{U} = (U, 0, 0)$ (see figure 2). One approximates furthermore the sphere by a paraboloid $h(r) \simeq h_0 + \frac{r^2}{2a}$, with r the distance to the axis of symmetry of the paraboloid (figure 6).

Under the lubrication assumptions [25], the Stokes equation (4) for the velocity field, $\underline{W} = (W_x, W_y, W_z)$, reduces to

$$\eta \frac{\partial^2 W_\parallel(x, y, z)}{\partial z^2} = \underline{\nabla}_\parallel P(x, y). \tag{25}$$
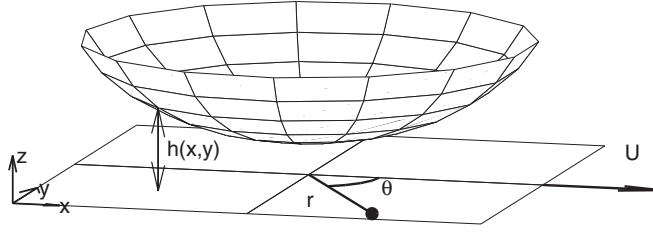
Figure 6. Flow description in the lubrication limit in the thin confined film.

The boundary conditions are written as

$$\frac{\partial W_x}{\partial z} = \frac{W_x - U}{\delta} \tag{26}$$

$$\frac{\partial W_y}{\partial z} = \frac{W_y}{\delta} \tag{27}$$

on the wall and

$$\underline{W} = \underline{0} \tag{28}$$

on the particle. These equations are easily integrated, and using the conservation equation $\underline{\nabla}_\parallel \cdot \underline{Q}_\parallel = 0$ for the flow rate, defined as $\underline{Q}_\parallel = \int_0^{h(x,y)} \underline{W}_\parallel \, \mathrm{d}z$, one gets the following equation for the pressure, P:

$$-\frac{1}{12\eta} \underline{\nabla}_\parallel \left(\frac{h^3(h + 4\delta)}{h + \delta} \underline{\nabla}_\parallel P \right) + \underline{U} \cdot \underline{\nabla}_\parallel \left(\frac{h^2}{2(h + \delta)} \right) = 0. \tag{29}$$

A general solution for the pressure can be written in the form $P = P_\infty + \Pi(r) \cos(\theta)$, with $\{r, \theta\}$ the angular coordinates on the planar wall. We could not, however, find an analytical solution for the previous differential equation. However, a 'heuristic solution' could be found after some manipulation of the differential equation in the form $\Pi(r) = \eta U \, r b[h(r)]$, with

$$b[h] = -\frac{6}{5h\delta} - \frac{9}{10} \frac{\ln(h)}{\delta^2} + \frac{4}{5} \frac{\ln(h + \delta)}{\delta^2} + \frac{1}{10} \frac{\ln(h + 4\delta)}{\delta^2}. \tag{30}$$

We refer to appendix A.2 for details of the calculations leading to this result. The validity of this approximate expression for the pressure was checked by computing numerically the solution of the full differential equation (29) using a simple ODE solver (Mathematica©). One finds that the previous solution for the pressure differs from the 'exact' numerical one by less than a few per cent for $\delta \in [0, R]$, $h_0 \in [\frac{R}{20}, R]$, and over the full range of distance $r \in [0, \infty[$ (see figure A.1 in the appendix). Moreover, in the vanishing slip length limit, $\delta \to 0$, the previous solution for $b[h]$ in equation (30) reduces to the corresponding exact solution of the differential equation, which can be easily obtained as $b_0(h) = -\frac{6}{5h^2}$.

Using this previous heuristic solution as a good approximation for the pressure, one may then write the force balance along the x-direction applied on the volume of fluid inside the cylinder $r < R_c$ (see figure 7) as

$$F_\mathcal{P} = - \left(F_{\text{wall}} + \int_{r=R_c} P \underline{n} \cdot \underline{x} \, \mathrm{d}S \right). \tag{31}$$

At large scales $R_c \to \infty$, one may verify that the slip effect disappears: $P(\delta, r = R_c) \to P(\delta = 0, r = R_c)$ and $\int_{r=R_c} P \, \mathrm{d}S$ is independent of δ and the dependence of the friction force acting on the particle P come from the $R_c \to \infty$ limit of F_{wall}.
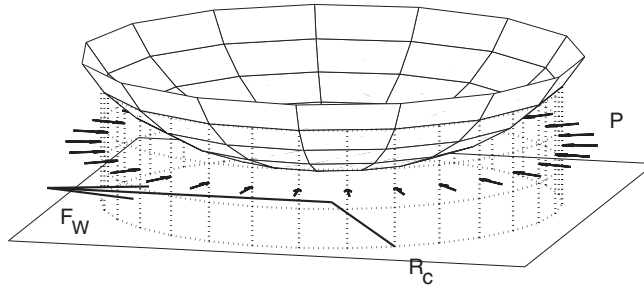
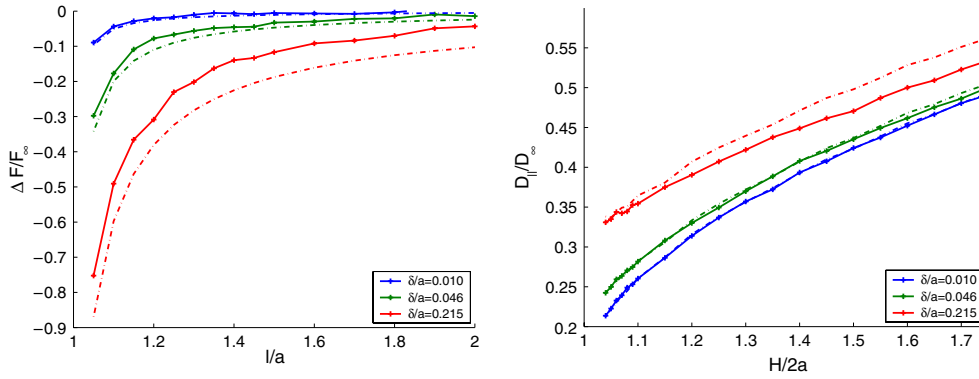**Figure 7.** Sketch of the force balance in the volume $r < R_c$.

Figure 8. Numerical test of the lubrication calculations: (left) plot of the friction force difference $\Delta F = F_{\text{wall}}(\delta) - F_{\text{wall}}(\delta = 0)$ normalized by the bulk value $F_\infty = 6\pi\eta a U$, for a single wall, as a function of the distance l to the wall. The solid line is the FEMLAB calculation, while the dashed line is the lubrication estimate; (right) diffusion coefficient for a particle in the middle plane of the confined geometry between two identical partially slipping walls, in the high confinement limit $H/2a \sim 1$. A good agreement between the numerical and lubrication calculations is found when $\delta \to 0$ and $H/2a \to 1$.

A second difficulty, however, arises with the lubrication calculation: whatever the slip length δ, the friction force on the wall, $F_{\text{wall}} = \int_{\text{wall}} \eta \nabla_\perp W_x \, dS$, is found to be logarithmically divergent when $R_c \to \infty$ [21]. This can be easily verified by inserting in the previous friction force expression the expression W_x deduced from the pressure field with equation (30) (see also equation (B.20) in appendix B). On the other hand, the *difference* of friction forces, $\Delta F_{\text{wall}} = F_{\text{wall}}[\delta] - F_{\text{wall}}[\delta = 0]$, between the finite slip length case and the no-slip case is found to take a finite value, given in equation (B.22). Note that $\Delta F_\mathcal{P} = \Delta F_{\text{wall}} \equiv \Delta F$ (since the second term in equation (31) is independent of δ in the $R_c \to \infty$ limit).

One may, however, argue that this difference is a physically relevant quantity since the slip effects mainly affect the flow in the region with strongest confinement. One may indeed verify that at the lubrication level, the flow with partial slip reduces to the flow with the no-slip boundary condition in the region far from closest contact.

We have plotted in figure 8 (left) the result for $\Delta F = F_{\text{wall}}[\delta] - F_{\text{wall}}[\delta = 0]$ (normalized by the bulk value of the force on the particle $F_\infty = 6\pi\eta a U$) as a function of the minimum gap h_0 between the sphere and the wall. This result is compared to the FEMLAB calculations in the same geometry. As expected, an agreement is found in the small gap limit, where the lubrication approximation is expected to be valid.
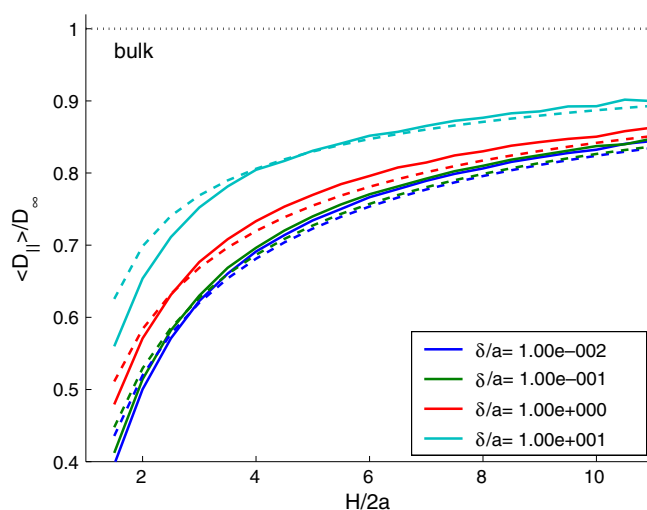
Figure 9. Mean diffusion coefficient between a no-slip wall and a partially slipping wall (δ) as a function of the gap H for various slip lengths δ. Full line: numerical results; dashed line: low confinement approximation (average of equation (24)).

Pursuing this calculation, a diffusion coefficient can be obtained. First the friction coefficient on the particle situated at a distance l from the wall (with slip length δ) can be estimated at this level of approximation by adding to the previous ΔF the value of the friction force $F_{\text{wall}}[l, \delta = 0]$ computed in the same configuration for a no-slip wall. Then the friction coefficient for the particle confined between two partially slipping walls is estimated by adding the effects of the walls on the friction coefficient, according to equation (23). The mobility is finally evaluated by the inverse of the friction coefficient. This procedure is applied in figure 8 (right), where the numerical (FEMLAB) result has been used for the no-slip friction force $F_{\text{wall}}[l, \delta = 0]$. Here the diffusion coefficient is computed only for the situation where the sphere is at the centre of the slab ($z = H/2$). This result is compared to 'exact' results obtained using a full FEMLAB calculation for the particle confined between two partially slipping walls. Again, the lubrication approximation only yields a correct agreement in the small gap region, and works better for small slip lengths. When the slip length increases, lubrication theory overestimates the mobility: in this case, important contributions to the viscous force are coming from areas far from the confined zones, which are not properly described within the lubrication approach.

The lubrication approach has therefore a quite limited range of application (in the very confined region) but the solution obtained is complementary to the low confinement result which works in the large gap limit.

6. Averaged diffusivity and conclusions

We are now in a position to compute the averaged diffusion coefficient over the confined slab, $\langle D_\parallel \rangle$ defined in equation (3). We consider a geometry where one wall is characterized by a no-slip boundary condition, while a partial slip boundary condition, with a slip length δ, applies on the other. This configuration is chosen so as to mimic the experimental geometry [19].

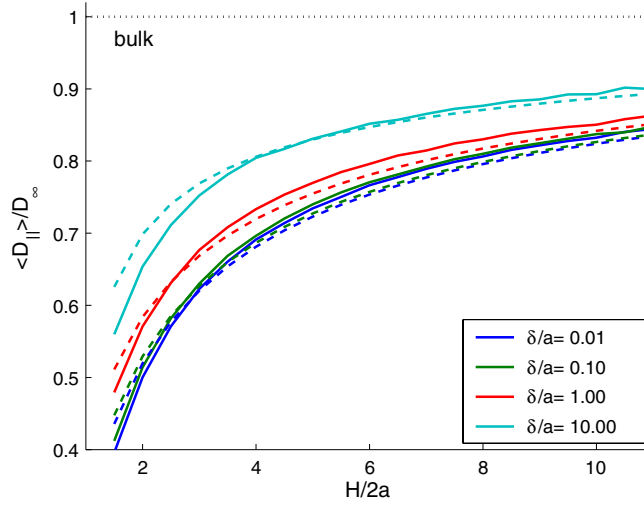Results are shown in figures 9 and 10 for various values of the confinement H and of the slip length δ.

Figure 10. Same as figure 9, but plotted as a function of slip length δ for fixed confinement H. Full line: numerical results; dashed line: low confinement approximation (average of equation (24)).

Analytical results obtained in the low confinement approximation, combined with the assumption of independent wall contribution, reproduce quite well the trends of the numerical computations. Figure 9 shows that the analytical estimate slightly underestimates diffusion in the low confinement limit, and tends to overestimate it at strong confinements.

In order to observe a significant dependence of diffusion on the slip length, two conditions are required. The particle size should not be much larger than the slip length, and a sufficiently strong confinement is required. With typical values of $H \simeq 4a$, variations of the average diffusion constant of typically 5% to 10% would be expected if the slip length is changed between $0.1a$ and a.

These results therefore suggest that diffusion measurements are quite sensitive to boundary conditions on the solid substrate. This opens new routes to measure slip length on the basis of the thermal motion of colloidal tracers [19].

Acknowledgment

Appendix A. First reflected field $\underline{V}^1$

A.1. Planar geometry

For a particle moving at a distance l from a planar surface, the general form of $\underline{V}^1$ satisfying equations (4)–(6) is given by [26]

$$V_x^1 = \frac{1}{2\pi} \int_0^\infty \int_0^{2\pi} \left[\left(2 - \cos^2(u)(k|z| + 1)\right) \Theta^1 + ik \cos(u) \Upsilon^1 + zk^2 \cos^2(u) \Xi^1 \right]$$
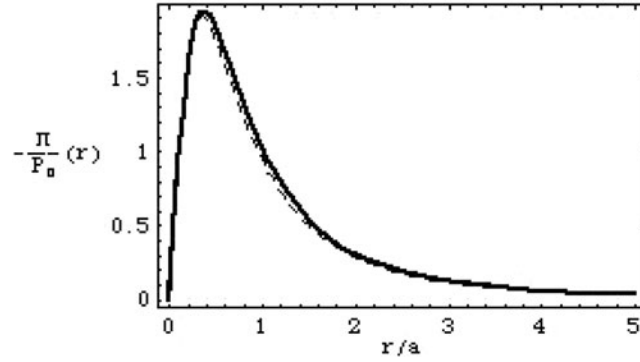$$\times e^{ik(x\cos(u)+y\sin(u))-k|z|} \, dk \, du \tag{A.1}$$

Figure A.1. Negative pressure $-\Pi(r) = -rb(r)$ rescaled by $P_0 = \eta U/a$, as a function of the radial distance r. The minimum gap h_0 between the sphere and the solid surface is $h_0 = 0.1a$ and the slip length is $\delta = a$. The solid line is the numerical solution of the equation for the pressure using an ODE solver (Mathematica©). The dashed line is the approximate solution, equation (B.18); see text.

$$V_y^1 = \frac{1}{2\pi} \int_0^\infty \int_0^{2\pi} i\sin(u) \left[i\cos(u)(k|z|+1)\Theta^1 + k\Upsilon^1 - izk^2\cos(u)\Xi^1 \right]$$
$$\times e^{ik(x\cos(u)+y\sin(u))-k|z|} \, dk \, du \tag{A.2}$$

$$V_z^1 = \frac{1}{2\pi} \int_0^\infty \int_0^{2\pi} \left[-izk\cos(u)\Theta^1 - k\Upsilon^1 + ik\cos(u)(k|z|+1)\Xi^1 \right]$$
$$\times e^{ik(x\cos(u)+y\sin(u))-k|z|} \, dk \, du \tag{A.3}$$

where Θ^1, Υ^1 and Ξ^1 are functions of k and u and (x, y, z) are Cartesian coordinates centred on the particle with x along the particle velocity and z normal to the wall.

The initial field $\underline{V}^0$ is written in this form with $(\Theta^0(k, u) = \frac{3}{4}aU$, $\Upsilon^0(k, u) = -\frac{1}{4}a^3 Uik\cos(u)$, $\Xi^0(k, u) = 0)$. In the limit of a small particle, $\Upsilon^0(k, u) \ll \Theta^0(k, u)$.

Functions $(\Theta^1, \Upsilon^1, \Xi^1)$ are determined as the unique solution of $\mathcal{BC}_\mathcal{S}(\underline{V}^0 + \underline{V}^1) = \underline{0}$:

$$\Theta^1 = \frac{3}{4} \frac{k\delta - 1}{k\delta + 1} aU e^{-2kl} \tag{A.4}$$

$$\Upsilon^1 = \frac{3i}{2} \frac{\left(2lk^2\delta^2 + k^2l^2\delta + k\delta l - \delta + kl^2 - l\right)}{2k^2\delta^2 + 1 + 3k\delta} Ua\cos(u) e^{-2kl} \tag{A.5}$$

$$\Xi^1 = -\frac{3}{2} \frac{(k\delta l + \delta + l)}{2k^2\delta^2 + 1 + 3k\delta} aU e^{-2kl}. \tag{A.6}$$

Integration of $V_x^1(0, 0, 0)$ gives

$$V_O^1 = -\frac{a}{l} C\left[\frac{l}{\delta}\right] U \tag{A.7}$$

with $C[y] = -\frac{3}{32}y^2 - \frac{9}{32}y - \frac{3}{8} + (\frac{3}{32}y^3 + \frac{3}{8}y^2 + \frac{3}{8}y)E(y) + \frac{3}{2}yE(2y)$. $E(y) = e^y Ei(1, y)$ and $Ei(1, y)$ is the exponential integral function.

A.2. Cylindrical geometry

For a particle moving in a cylinder, the general solution for the reflected field $\underline{V}^1$ in (r, ϕ, z) cylindrical coordinates is

$$\underline{V}^1(r, \phi, z) = \frac{3aU}{2\pi} \sum_{k=-\infty}^{+\infty} \int_0^{+\infty} d\lambda \begin{pmatrix} a_k(\lambda, r) \cos(k\phi) \sin(\lambda z) \\ b_k(\lambda, r) \sin(k\phi) \sin(\lambda z) \\ c_k(\lambda, r) \cos(k\phi) \cos(\lambda z) \end{pmatrix}_{(\underline{e}_r, \underline{e}_\phi, \underline{e}_z)} \tag{A.8}$$

$$a_k(\lambda, r) = \frac{k}{\lambda r} \Omega_k^1(\lambda) I_k(\lambda r) + \Psi_k^1(\lambda) I_k'(\lambda r) + \lambda r \Pi_k^1(\lambda) I_k''(\lambda r)$$

$$b_k(\lambda, r) = -\Omega_k^1(\lambda) I_k'(\lambda r) - \frac{k}{\lambda r} \Psi_k^1(\lambda) I_k(\lambda r) - k\Pi_k^1(\lambda) I_k'(\lambda r) + \frac{k}{\lambda r} \Pi_k^1(\lambda) I_k(\lambda r) \tag{A.9}$$

$$c_k(\lambda, r) = \Psi_k^1(\lambda) I_k(\lambda r) + \lambda r \Pi_k^1(\lambda) I_k'(\lambda r) + \Pi_k^1(\lambda) I_k(\lambda r)$$

where I_k, I_k' and I_k'' are the first-order modified Bessel functions and their derivatives.

The bulk field $\underline{V}^0$ for a particle moving along the cylinder axis, at a distance b from it, is expressed in such a form as

$$\underline{V}^0(r, \phi, z) = \frac{3aU}{2\pi} \sum_{k=-\infty}^{+\infty} \int_0^{+\infty} d\lambda \begin{pmatrix} \alpha_k(\lambda, r) \cos(k\phi) \sin(\lambda z) \\ \beta_k(\lambda, r) \sin(k\phi) \sin(\lambda z) \\ \gamma_k(\lambda, r) \cos(k\phi) \cos(\lambda z) \end{pmatrix}_{(\underline{e}_r, \underline{e}_\phi, \underline{e}_z)} \tag{A.10}$$

$$\alpha_k(\lambda, r) = \left(\lambda r + \frac{k^2}{\lambda r}\right) K_k(\lambda r) I_k(\lambda b) + \lambda b K_k'(\lambda r) I_k'(\lambda b)$$

$$\beta_k(\lambda, r) = -k\left(K_k'(\lambda r) I_k(\lambda b) + \frac{b}{r} K_k(\lambda r) I_k'(\lambda b)\right) \tag{A.11}$$

$$\gamma_k(\lambda, r) = 2K_k(\lambda r) I_k(\lambda b) + \lambda r K_k'(\lambda r) I_k(\lambda b) + \lambda b K_k(\lambda r) I_k'(\lambda b)$$

where K_k, K_k' and K_k'' are the second-order modified Bessel functions and their derivatives.

$\Omega_k^1(\lambda)$, $\Psi_k^1(\lambda)$ and $\Pi_k^1(\lambda)$ are the unique solution of

$$\mathcal{BC}_S(\underline{V}^0 + \underline{V}^1) = \underline{0} \tag{A.12}$$

on the cylindrical wall $r = R$. The analytical expression is then used to compute numerically $V_{\mathcal{P}}^1$ as

$$V_{\mathcal{O}}^1 = \frac{3aU}{2\pi} \sum_{k=-\infty}^{+\infty} \int_0^{+\infty} \left[(\Psi_k(\lambda) + \Pi_k(\lambda)) I_k(\lambda b) + \mu b \Pi_k(\lambda) I_k'(\lambda b)\right] d\lambda. \tag{A.13}$$

Appendix B. Lubrication approximation

Using reduced variables $r = \sqrt{2h_0 a}\tilde{r}$, $h = h_0\tilde{h}$, $\delta = h_0\tilde{\delta}$ and $P = \eta U \frac{\sqrt{2h_0 a}}{h_0^2}\tilde{p}$, mass conservation is (for compactness we remove the $\tilde{\ }$ for the reduced variables):

$$-\underline{\nabla}_\| \left(\frac{h^3(h + 4\delta)}{12(h + \delta)}\underline{\nabla}_\| p\right) + \underline{e}_x \cdot \underline{\nabla}_\| \left(\frac{h^2}{2(h + \delta)}\right) = 0 \tag{B.14}$$

with $h(r) = 1 + r^2$.

Assuming $p(r) = p_\infty + rb(r)\cos(\theta)$, equation (B.14) becomes

$$-\frac{\partial}{\partial r}\left[r\alpha(h(r))\frac{\partial}{\partial r}(rb(r))\right] + \alpha(h(r))b(r) + 2r\beta(h(r)) = 0 \tag{B.15}$$

with $\alpha(h) = \frac{h^3(h + 4\delta)}{12(h + \delta)}$ and $\beta(h) = \frac{h^2 + 2\delta h}{2(h + \delta)^2}$.

We could not find an exact solution for this equation. However, in order to proceed further, we have tried to construct in a heuristic way a good approximation to the solution to

avoid purely numerical solutions. We have proceeded as follows. First b is assumed to depend functionally on $h(r)$, as $b[h(r)]$. Expressing $p = P_\infty + xb[h]$ ($x = r\cos\theta$) in equation (B.14), this equation rewrites as

$$-\underline{\nabla}_\parallel \cdot \left(\alpha(h) \left(b(h)\underline{e}_x + x\frac{\partial b}{\partial h}\underline{\nabla}_\parallel h \right) \right) + 2\beta(h)x = 0 \tag{B.16}$$

with $\underline{\nabla}_\parallel h = \{2x, 2y\}$ in Cartesian coordinates. A heuristic solution is found by assuming $\alpha(h)$, $\beta(h)$ and $\frac{\partial b}{\partial h}$ as constant in the previous equation, which amounts to replacing the previous equation by

$$-6x\frac{\partial b}{\partial h} + 2\mathcal{A}\beta(h)x = 0. \tag{B.17}$$

The constant $\mathcal{A}$ is adjusted so that the exact no-slip solution of equation (B.14), $b_0(h) = -\frac{6}{5h^2}$, is recovered. The solution of equation (B.17) with $\mathcal{A} = 6/5$ is

$$b(h) = -\frac{6}{5h\delta} - \frac{9}{10}\frac{\ln(h)}{\delta^2} + \frac{4}{5}\frac{\ln(h+\delta)}{\delta^2} + \frac{1}{10}\frac{\ln(h+4\delta)}{\delta^2}, \tag{B.18}$$

which indeed reduces to the no-slip solution $b_0(h) = -\frac{6}{5h^2}$ when $\delta \to 0$. Note also that in the limit $h \gg \delta$, one also recovers $b(h) \to b_0(h)$: the pressure is independent of δ far from the particle.

The reduced viscous force acting on the wall is

$$F_{\text{wall}} = \int \frac{\partial W_x}{\partial z} r \, \mathrm{d}r \, \mathrm{d}\theta. \tag{B.19}$$

W_x is determined from Stokes equation $\frac{\partial^2 W_x}{\partial z^2} = \frac{\partial p}{\partial x}$ along with the boundary conditions and yields

$$F_{\text{wall}} = 3\pi \int_0^\infty \left[\frac{1}{6}(b(r) + \frac{\partial}{\partial r}(rb(r)))\frac{h^2}{h+\delta} + \frac{2}{3}\frac{1}{h+\delta} \right] r \, \mathrm{d}r + \text{constant.} \tag{B.20}$$

Deviation of the viscous force from $\delta = 0$ case is, back with dimensionalized variables,

$$\Delta F = 6\pi\eta aU \int_0^\infty \left[\frac{h-1}{6}\left(b_0(h) - b(h)\frac{h(h+2\delta)}{(h+\delta)^2}\right) - \frac{2}{6}\frac{\delta}{h(h+\delta)} \right] \mathrm{d}h. \tag{B.21}$$

This expression can be exactly computed for the approximated $b(h)$ given above:

$$\begin{aligned} \Delta F = \frac{6\pi\eta aU}{360\delta^2} \Bigg(& 36\delta - 12\delta^2 + 10\pi^2\delta^2 + 54\delta\ln\left(\frac{1}{\delta}\right) - 54\delta^2\ln\left(\frac{1}{\delta}\right) \\ & + 27\delta^2\ln\left(\frac{1}{\delta}\right)^2 + 3\delta^2\ln\left(\frac{1}{3\delta}\right)^2 - 24\ln(1+\delta) + 134\delta\ln(1+\delta) \\ & - 190\delta^2\ln(1+\delta) - 24\delta^2\ln(1+\delta)^2 - 54\delta\ln\left(\frac{1+\delta}{\delta}\right) + 54\delta^2\ln\left(\frac{1+\delta}{\delta}\right) \\ & - 3\ln(1+4\delta) - 26\delta\ln(1+4\delta) - 56\delta^2\ln(1+4\delta) \\ & - 6\delta^2\ln(1+\delta)\ln(1+4\delta) + 6\delta^2\ln(1+\delta)\ln\left(\frac{1+4\delta}{3\delta}\right) \\ & + 54\delta^2\text{Li}_2\left[\frac{-1}{\delta}\right] + 6\delta^2\text{Li}_2\left[\frac{-1-\delta}{3\delta}\right] \Bigg) \end{aligned} \tag{B.22}$$

with $\text{Li}_2(x)$ the dilogarithm function defined as $\text{Li}_2(z) = \sum_{k=1,\infty} z^k/k^2$.[3]

---

[3] Note that this definition is slightly changed from that in [22] where it is defined as $\tilde{\text{Li}}_2(z) = \sum_{k=1,\infty}(-1)^k(z - 1)^k/k^2$.

References

[1] Granick S, Zhu Y and Hyunjung L 2003 *Nat. Mater.* **2** 221
[2] Cottin-Bizonne C, Cross B, Steinberger A and Charlaix E 2005 *Phys. Rev. Lett.* **94** 056102
[3] Richarson S 1973 *J. Fluid Mech.* **59** 707
[4] Lauga E, Brenner M and Stone H 2005 Microfluidics: the no-slip boundary condition *Handbook of Experimental Fluid Dynamics* ed J Foss, C Tropea and A Yarin (Berlin: Springer) at press
[5] Bocquet L and Barrat J-L 1994 *Phys. Rev.* E **49** 3079
[6] Andrienko D, Dunweg B and Vinogradova O I 2003 *J. Chem. Phys.* **119** 13106
[7] Cieplak M, Koplik J and Banavar J R 2001 *Phys. Rev. Lett.* **86** 803
[8] Bocquet L and Barrat J-L 1999 *Phys. Rev. Lett.* **82** 4671
[9] Sokhan V P, Nicholson D and Quirke N 2001 *J. Chem. Phys.* **115** 3878
[10] Watanabe K, Udagawa Y and Udagawa H 1999 *J. Fluid Mech.* **381** 225
[11] Pit R, Hervet H and Leger L 2000 *Phys. Rev. Lett.* **85** 980
[12] Cottin-Bizonne C, Charlaix E, Bocquet L and Barrat J-L 2003 *Nat. Mater.* **2** 238
[13] Cottin-Bizonne C, Barentin C, Charlaix E, Bocquet L and Barrat J-L 2004 *Eur. Phys. J.* E **15** 427
[14] Ou J, Perot B and Rothstein J P 2004 *Phys. Fluids* **16** 4635
[15] Tretheway D C and Meinhart C D 2002 *Phys. Fluids* **14** 9
[16] Craig V, Neto C and Williams D 2001 *Phys. Rev. Lett.* **87** 054504
[17] Bechoefer J, Géminard J-C, Bocquet L and Oswald P 1997 *Phys. Rev. Lett.* **79** 4922
[18] Alméras Y, Barrat J-L and Bocquet L 2000 *J. Physique Coll.* **10** 27
[19] Joly L, Ybert C and Bocquet L 2005 *Preprint* cond-mat/0507054
[20] Einstein A 1905 *Ann. Phys., Lpz.* **17** 549
[21] Happel J and Brenner H 1973 *Low Reynolds Number Hydrodynamics* (Dordrecht: Kluwer)
[22] Abramowitz M and Stegun I A 1965 *Handbook of Mathematical Functions* (New York: Dover)
[23] Lauga E and Squires T M 2005 Brownian motion near a partial slip boundary, a local probe of the no-slip condition *Preprint* cond-mat/0506212
[24] Faxen H 1924 *Ark. Mat. Astron. Fys.* **18** 1
[25] Batchelor G K 1973 *An Introduction to Fluid Dynamics* (Cambridge: Cambridge University Press)
[26] Morse P and Feshbach H 1953 *Methods of Theoretical Physics* (New York: McGraw-Hill)